Realistic simulated lung nodule dataset for testing CAD detection and sizing

Robert D. Ambrosini[1] and Walter G. O'Dell[1,2]

Departments of [1]Biomedical Engineering and [2]Radiation Oncology, University of Rochester, Rochester, NY 14642-8647, USA

ABSTRACT

The development of computer-aided diagnosis (CAD) methods for the processing of CT lung scans continues to become increasingly popular due to the potential of these algorithms to reduce image reading time, errors caused by user fatigue, and user subjectivity when screening for the presence of malignant lesions. This study seeks to address the critical need for a realistic simulated lung nodule CT image dataset based on real tumor morphologies that can be used for the quantitative evaluation and comparison of these CAD algorithms. The manual contouring of 17 different lung metastases was performed and reconstruction of the full 3-D surface of each tumor was achieved through the utilization of an analytical equation comprised of a spherical harmonics series. 2-D nodule slice representations were then computed based on these analytical equations to produce realistic simulated nodules that can be inserted into CT datasets with well-circumscribed, vascularized, or juxtapleural borders and also be scaled to represent nodule growth. The 3-D shape and intensity profile of each simulated nodule created from the spherical harmonics reconstruction was compared to the real patient CT lung metastasis from which its contour points were derived through the calculation of a 3-D correlation coefficient, producing an average value of 0.8897 (±0.0609). This database of realistic simulated nodules can fulfill the need for a reproducible and reliable gold standard for CAD algorithms with regards to nodule detection and sizing, especially given its virtually unlimited capacity for expansion to other nodule shape variants, organ systems, and imaging modalities.

Keywords: Lung nodules, CAD validation, spherical harmonics

1. INTRODUCTION

Recent advances in treatment, such as those seen with stereotactic radiosurgery and radiotherapy techniques[1-8], have resulted in renewed motivation for the detection and diagnosis of small lesions in the lung, especially in regards to surveillance for metastatic disease to the lung in high-risk patient populations with primary cancer of the breast, colon, bladder, and kidney. However, multi-detector CT scanners typically generate 300 to 600 image slices and the reading and interpretation of these massive amounts of image data require a tremendous level of radiologist effort, predisposing the screening process to human error. Swensen et al. found that when expert human readers performed retrospective interpretation of baseline CT lung images, nodules were found to have been missed initially in 26% of patients[9]. A chief concern is the detection of nodules of small size, low contrast, or those located near vessel structures, since these nodules are often missed by the unaided radiologist[10]. Thus, computer-aided diagnosis (CAD) approaches are becoming increasingly necessary for both reducing radiologists' effort and improving detection sensitivity of early stage lung disease.

As the potential of CAD systems for providing accurate and efficient nodule detection and sizing continues to be realized, the availability of appropriate validation datasets becomes increasingly necessary. The Lung Image Database Consortium (LIDC) and Early Lung Cancer Action Project (ELCAP) studies sought to employ real patient CT datasets as standards for comparisons of competing CAD methods for the detection of suspicious lung nodules[11-14]. However, both studies found a surprisingly large variation in their readers' definitions of ground truth that is likely to mask any real differences in performance of most CAD schemes, thereby negating the usefulness of these databases. Likewise, there was tremendous disagreement among the LIDC reviewers in their estimates of nodule volume, thwarting

Medical Imaging 2010: Computer-Aided Diagnosis, edited by Nico Karssemeijer, Ronald M. Summers,
Proc. of SPIE Vol. 7624, 76242X · © 2010 SPIE · CCC code: 1605-7422/10/$18 · doi: 10.1117/12.843996

the use of these datasets for comparison of automated approaches for quantifying tumor size and growth[15]. For the average nodule diameter size of 7.05 mm, the 95% confidence interval in volume estimates spanned a 16-fold uncertainty range. This degree of variability suggests that human interpretation of real patient datasets cannot be used alone as ground truth and motivates the creation of synthetic nodule datasets where the ground truth for size and growth is known implicitly.

Although the addition of synthetic nodules to lung phantoms is one commonly employed option for constructing simulated nodule datasets, the lack of patient motion artifacts, appropriately complex nodule borders, and sufficiently detailed surrounding anatomy prevents the confident extrapolation of phantom study results to clinical use[16]. On the other hand, simulated nodule dataset creation through the insertion of computer-generated simulated nodules into medical images has the potential to circumvent these weaknesses while offering a high degree of flexibility for CAD validation. However, prior simulated datasets based around the addition of computer-generated nodules to lung CT image data have often involved the use of simple geometric shapes such as spheres or ellipsoids that are either inserted as symmetric 3-D objects or transformed into non-symmetric objects through random shape manipulations. For example, Zhang et al. created non-symmetric synthetic nodules consisting of a sphere with random surface fluctuations[17]. A major issue with these approaches to simulated dataset construction is that they lack sufficient biological motivation for their simulated nodule 3-D geometries. Some approaches have involved modeling simulated nodule shapes after real lung nodule data[18-19], however the goal in these studies has been to create simulated nodules that emulate the characteristics of real nodules, not necessarily the re-construction of the 3-D morphologies of the individual real lung nodules such that they can then be thoroughly manipulated and inserted into new medical images as the simulated nodules. Furthermore, it is important in creating simulated nodule datasets for lung nodules to include a representative proportion of vascularized and juxtapleural nodules that historically have provided the greatest challenge for CAD systems and human readers alike[10, 20]. Consequently, the testing of CAD approaches to such datasets produces results that are not particularly meaningful for extrapolation to outcomes on real patient data.

We propose to create a realistic simulated lung nodule image dataset that overcomes the aforementioned limitations in order to provide a basis for future comparison of CAD and human readers for both detection and sizing of nodules. Unlike prior work, our synthetic database is constructed with nodule shapes derived from real patient lung lesions, employs mathematically scaled versions of each nodule so as to enable the true assessment of nodule growth, and permits vascularized and juxtapleural nodules in proportions representative of the patterns of occurrence found in large patient datasets.

2. METHODS

In order to provide an objective and adaptable system to validate the accuracy of lung nodule CAD detection and sizing algorithms, we have designed a synthetic nodule image dataset consisting of isolated nodules. For the purpose of constructing this dataset, a total of 17 confirmed lung metastases, ranging in diameter from approximately 8 to 20 millimeters, were contoured manually from four different patient CT datasets (slice thickness and separation of 3 mm and in-plane resolution of 0.9375 mm). This contouring process generated roughly 150 to 500 unique surface points for each patient nodule. An analytical equation comprised of a spherical harmonic series was then used to reconstruct the full 3-D surface of each tumor:

$$r = \sum_{l=0}^{3} \sum_{m=-l}^{l} A_{l,m}\, Y_l^m(\theta,\phi)$$

$$Y_l^m(\theta,\phi) = \sqrt{\frac{2l+1}{4\pi}\frac{(l-m)!}{(l+m)!}}\, P_l^m(\cos\theta)\, e^{im\phi} \qquad (1)$$

where r is the nodule radius, A represents the constants determined from the extracted nodule contouring, Y is the spherical harmonic, θ is the polar (colatitudinal) coordinate, ϕ is the azimuthal (longitudinal) coordinate, and P is an associated Legendre polynomial. Through the utilization of the analytical equation, a high-resolution surface mesh was

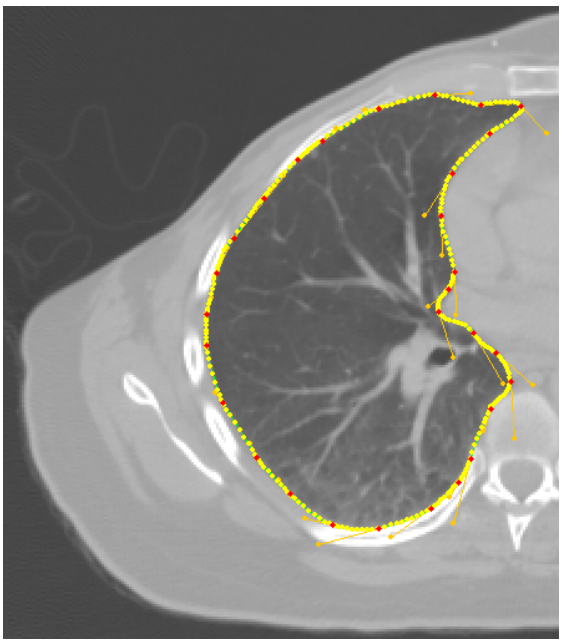

Figure 1. Display of semi-automated snake that was utilized for contouring of CT lung slices during construction of juxtapleural simulated nodules. Example image slice is shown with snake placed along CT lung outer edge where red points along contour are control points, yellow points along contour are automatically generated interpolation points, and orange wands are used for adjusting control point slopes.

created that allowed an exact computation of each nodule's true volume. Furthermore, this surface mesh also enabled the 3-D reconstruction of the appearance of each nodule, subjected to any degree of size scaling, under any set of voxel dimensions.

The appearance of each simulated nodule on a series of CT image slices was achieved through a sequence of steps. First, the eventual central coordinate of each nodule within the 3-D lung space of the designated insertion CT dataset was determined, with precision equal to 0.1 of the voxel dimension in each direction. Thus, nodules were not merely centered on a given pixel and the positions of different nodules were not identically centered. The 2-D nodule slice representations were computed assuming a uniform nodule density (matched to the intensity of the insertion dataset blood signal) where relative voxel intensities were based upon the partial volume of the nodule in each voxel. In the

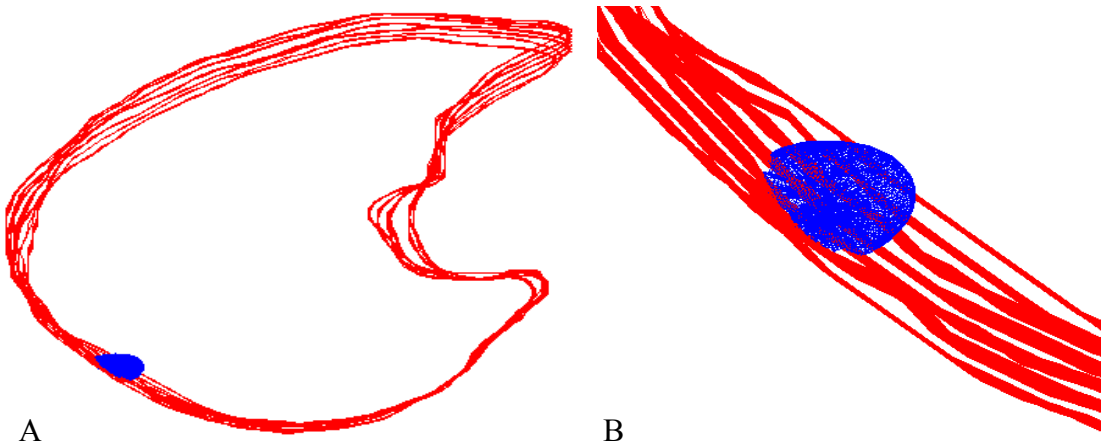

Figure 2. Example reconstruction of one of the 17 extracted CT lung metastases where boundary constraints provided by adjacent lung contour data result in a juxtapleural border profile of the reconstructed nodule. In [A], the reconstructed nodule is shown with the complete surrounding lung contour data from the multiple CT lung slices adjacent to its eventual point of insertion. In [B], the same reconstructed nodule is shown in closer detail where only the lung contour data in the immediate vicinity of the nodule reconstruction is visible. 3-D surface contour points of the nodule were generated through the use of spherical harmonics equations while lung contours were derived from semi-automated contouring of CT lung image data.

Simulated Nodule	3-D Correlation Coefficient
1	0.8906
2	0.9237
3	0.9390
4	0.7605
5	0.9224
6	0.8854
7	0.8902
8	0.7139
9	0.9129
10	0.9323
11	0.9160
12	0.8640
13	0.9104
14	0.9075
15	0.9141
16	0.9248
17	0.9168
	0.8897 (± 0.0609)

Table 1. 3-D correlation coefficient values calculated between 17 individual simulated nodules generated from spherical harmonics-based 3-D shape reconstructions and the corresponding real patient CT lung nodules.

process of simulated nodule insertion, the prevention of unrealistically bright voxels was achieved by using the maximum intensity between the simulated nodule and the background features of the insertion dataset, rather than the sum of intensities, in each overlapping voxel. The use of maximal intensity allowed us to preserve background features such that both nodules and vessels could share the same pixels. The point spread function of a standard clinical imaging scanner was then replicated through blurring of the simulated nodule and its neighboring voxels with a Gaussian filter. Lastly, Gaussian noise was added utilizing a standard deviation derived from the average noise inherent within the employed patient CT datasets.

During a review of their database of 200 pulmonary nodules, Kostis and his group found that almost half of all nodules were vascularized, around one-third had well-circumscribed boundaries, and approaching one-quarter of all nodules were juxtapleural[21]. The fourth class, nodules with pleural tails, was found to be present in only about 1% of the nodules in the database and as such, are assumed to represent a considerable rarity among pulmonary nodules. In order to account for the three major classes of lung nodule border profiles, the complete database of simulated nodules was implemented and tested in all three different manifestations. Well-circumscribed simulated nodules were constructed as detailed above and then inserted into a region of a healthy patient CT dataset where no overlap was permitted between the voxels of the inserted nodule and blood vessel or lung wall voxels of comparable brightness. Vascularized simulated nodules involved an identical design procedure as performed with the well-circumscribed simulated nodule versions, however they were inserted deliberately at a large vessel bifurcation and allowed to share voxels with the background blood vessels to generate realistically the scenario where both structures are located within the same (3 – 7 mm thick) CT image slice. As far as juxtapleural simulated nodules, the effects of growth along the lung pleural surface on the nodule's 3-D shape was incorporated into the creation process during the 3-D nodule reconstruction process itself to ensure that a correct gold standard volume was still calculated for the adjusted shape. The lung slice contours for the insertion CT dataset were extracted using a semi-automatic snake implementation designed by our lab and built upon the NIH's ImageJ platform (see Figure 1). A solid 3-D lung mask was generated through a process of simple interpolation in-between extracted slices and once an insertion point within the lung had been selected, the spatial coordinates provided by the lung mask were combined with the spatial coordinates of the simulated nodules' reconstruction to produce a juxtapleural simulated nodule (see Figure 2). Through the use of this style of juxtapleural nodule creation, a progressive increase in scaling size for a given 3-D shape led to the replication of the appearance of nodule growth adjacent to and outward from the lung wall.

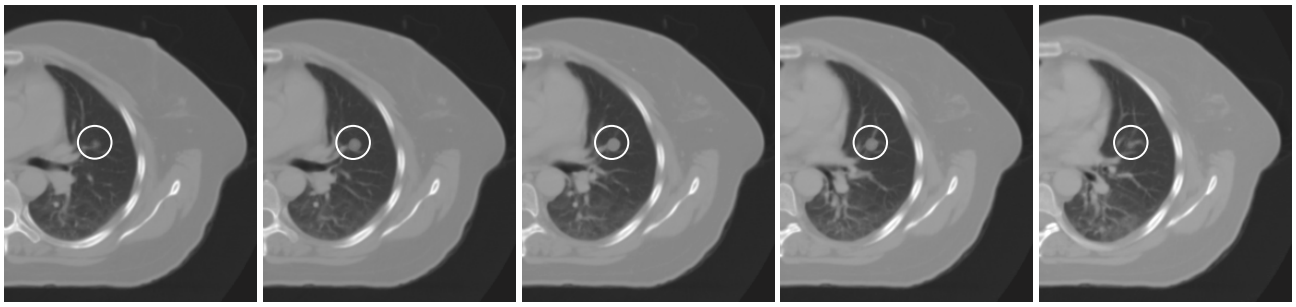

Figure 3. Five sequential CT slices illustrating the insertion of a simulated nodule (circled) with a vascularized border profile.

3. RESULTS

A critical aspect of this work was establishing the degree of similarity between our simulated nodules that were produced through the spherical harmonics-based 3-D reconstructions and the real patient lung nodules that were extracted manually to provide the 3-D contour points utilized as the source data for the reconstruction process. Each individual simulated nodule was compared to the corresponding real patient lung nodule that was used as the basis for its construction through the calculation of a 3-D correlation coefficient. A 3-D correlation coefficient was selected as the means of establishing the accuracy of our spherical harmonics-based 3-D nodule reconstructions due to its capacity as a similarity measure to incorporate a simultaneous comparison between both the 3-D shape and the 3-D relative intensity profile of each simulated nodule and the contoured real nodule that was used as its source data. For the 17 simulated-to-real nodule comparisons, an average 3-D correlation coefficient value of 0.8897 with a standard deviation of 0.0609 was calculated (see Table 1). This high quantitative correlation signifies that the generated simulated nodules possess both realistic 3-D morphologies and intensity profiles.

In order to have confidence in a lung nodule CAD algorithm, the applied method must show the capability to handle effectively vascularized and juxtapleural boundary conditions, in addition to well-circumscribed margins, as these are also common lung nodule presentations. Consequently, the other vital point of analysis for our system was its capacity to produce simulated nodules with realistic boundary presentations. The sequential CT slice appearance of a sample vascularized simulated nodule is shown in Figure 3 while the sequential CT slice appearance of a sample juxtapleural simulated nodule is displayed in Figure 4. These examples demonstrate that our approach does in fact generate nodules within CT datasets that simulate realistically the challenging presentation of vascularized and juxtapleural nodules for CAD algorithm testing.

4. CONCLUSIONS

In this paper, a novel system for constructing a database of simulated nodules with realistic 3-D shapes, intensity profiles, and either well-circumscribed, vascularized, or juxtapleural borders is presented. A critical aspect of this work is the quantitative assessment of the similarity between the 3-D shape and intensity profile of each initially generated simulated nodule and the corresponding manually contoured real lung nodule on which it was based. The 3-D correlation coefficient values and the simulated nodule appearance results presented in this work indicate that our system of spherical harmonics-based 3-D reconstructions provides simulated nodules with realistic 3-D shapes, borders, and intensity profiles that can be utilized to assess the detection and sizing capabilities of any CT lung nodule CAD approach. This positive outcome is the result of utilizing real lung nodule morphologies for generating the nodule shapes and using accurate partial volume effects and image features of blur and noise to generate the CT appearance. Moreover, we have previously shown the ability of our system to scale each nodule at a wide range of percentages from its original volume, further illustrating the flexibility and effectiveness of our system as a means for generating a highly adaptable simulated nodule dataset[22].

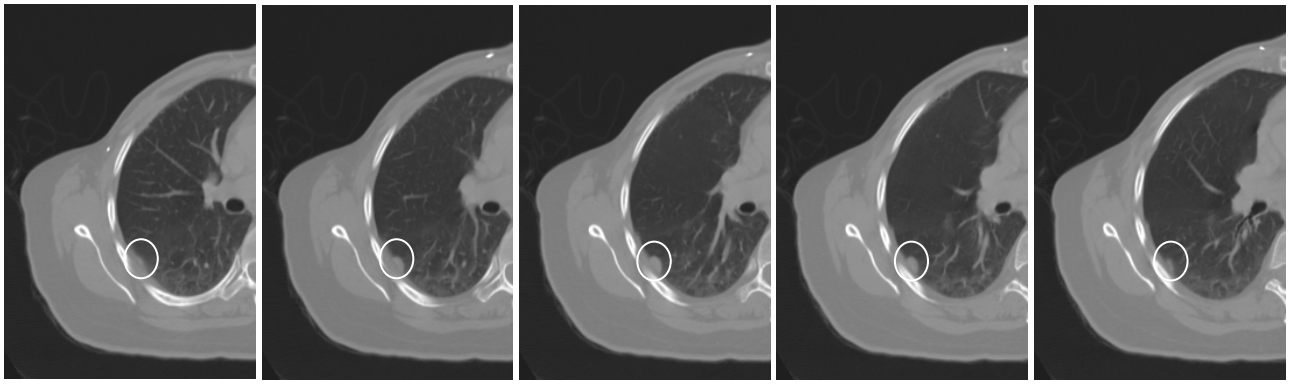

Figure 4. Five sequential CT slices illustrating the insertion of a simulated nodule (circled) with a juxtapleural border profile.

One limitation of the work presented in this paper was the level of user involvement that was required for simulated nodule generation and insertion into CT image data. For example, the location of each vascularized simulated nodule was selected manually in order to ensure that it was placed sufficiently adjacent to a prominent pulmonary vessel. In future implementations of our system, the efficient placing of vascularized nodules randomly throughout the CT lung space that are constrained such that they share borders with sizable vessels will be facilitated through the introduction of a vessel tree segmentation step. This segmentation of lung vessels will be achieved through the use of a labeled 3-D flood-fill operation that has been developed by one of the co-authors. Along the same lines, the automatic and random placement of juxtapleural simulated nodules around the lung-chest wall interface will be achieved through the application of an automatic lung surface extraction program demonstrated previously by one of the co-authors and colleagues[23].

The simulated datasets utilized for Figures 3 and 4 employed the same patient CT image data as the background for all simulated nodules. In order to improve the diversity and applicability of our simulated nodule datasets, a major area of future work will be the obtaining of additional baseline patient datasets from the LIDC database for use as background CT image data. Reportedly, over 500 LIDC datasets have been collected by the LIDC teams that are either currently available or that will soon be made available to the public[24]. Only those datasets where all four LIDC reviewers found no lesions, or at least the fewest contentious lesions among the available data sets (least variable interpretation among the four reviewers) will be selected so as to ensure that no true candidate nodules except for the simulated ones are used to provide a basis for the assessment of detection sensitivity and the number of false positives. In addition, emphasis will be placed on selecting datasets from the LIDC database that have varying image parameters such as slice thickness, in-plane pixel dimensions, and signal-to-noise ratios to further enrich the quality of our simulated image database. Along these same lines, planned extensions of this work will also include the development of a web-based interface that would allow the dissemination of simulated image datasets and the uploading of user results for the automatic determination of standardized error metrics, as well as the expansion of the simulated nodule database through the incorporation of a greater number of 3-D real patient nodule reconstructions.

ACKNOWLEGDMENTS

Robert Ambrosini is a trainee in the Medical Scientist Training Program, NIH T32 GM-07356.

REFERENCES

[1] Okunieff, P., Petersen, A.L., Philip, A., Milano, M.T., Katz, A.W., Boros, L., and Schell, M.C., "Stereotactic body radiation therapy (SBRT) for lung metastases," Acta Oncol. 45(7), 808-817 (2006).
[2] Kavanagh, B.D., McGarry, R.C., and Timmerman, R.D., "Extracranial radiosurgery (stereotactic body radiation therapy) for oligometastases," Semin. Radiat. Oncol. 16(2), 77-84 (2006).

[3] Aoki, M., Abe, Y., Kondo, H., Hatayama, Y., Kawaguchi, H., Fujimori, A., Suzaki, K., Seino, M., Morita, T., Souma, M., Tsushima, T., and Takanashi, S., "Clinical outcome of stereotactic body radiotherapy of 54 Gy in nine fractions for patients with localized lung tumor using a custom-made immobilization system," Radiat. Med. 25(6), 289-294 (2007).
[4] Guckenberger, M., Heilman, K., Wulf, J., Mueller, G., Beckmann, G., and Flentje, M., "Pulmonary injury and tumor response after stereotactic body radiotherapy (SBRT): results of a serial follow-up CT study," Radiother. Oncol. 85(3), 435-442 (2007).
[5] Norihisa, Y., Nagata, Y., Takayama, K., Matsuo, Y., Sakamoto, T., Sakamoto, M., Mizowaki, T., Yano, S., and Hiraoka, M., "Stereotactic body radiotherapy for oligometastatic lung tumors," Int. J. Radiat. Oncol. Biol. Phys. 72(2), 398-403 (2008).
[6] Coon, D., Gokhale, A.S., Burton, S.A., Heron, D.E., Ozhasoglu, C., and Christie, N., "Fractionated stereotactic body radiation therapy in the treatment of primary, recurrent, and metastatic lung tumors: the role of positron emission tomography/computed tomography-based treatment planning," Clin. Lung Cancer 9(4), 217-221 (2008).
[7] Guckenberger, M., Wulf, J., Mueller, G., Krieger, T., Baier, K., Gabor, M., Richter, A., Wilbert, J., and Flentje, M., "Dose-response relationship for image-guided stereotactic body radiotherapy of pulmonary tumors: relevance of 4D dose calculation," Int. J. Radiat. Oncol. Biol. Phys. 74(1), 47-54 (2009).
[8] Rusthoven, K.E., Kavanagh, B.D., Burri, S.H., Chen, C., Cardenes, H., Chidel, M.A., Pugh, T.J., Kane, M., Gaspar, L.E., and Schefter, T.E., "Multi-institutional phase I/II trial of stereotactic body radiation therapy for lung metastases," J. Clin. Oncol. 27(10), 1579-1584 2009.
[9] Swensen, S.J., Jett, J.R., Sloan, J.A., Midthun, D.E., Hartman, T.E., Sykes, A.M., Aughenbaugh, G.L., Zink, F.E., Hillman, S.L., Noetzel, G.R., Marks, R.S., Clayton, A.C., and Pairolero, P.C., "Screening for lung cancer with low-dose spiral computed tomography," Am. J. Respir. Crit. Care. Med. 165(4), 508-513 (2002).
[10] Kakinuma, R., Ohmatsu, H., Kaneko, M., Eguchi, K., Naruke, T., Nagai, K., Nishiwaki, Y., Suzuki, A., and Moriyama, N., "Detection failures in spiral CT screenings for lung cancer: analysis of CT findings," Radiology 212(1), 61-66 (1999).
[11] Clarke, L.P., Croft, B.Y., Staab, E., Baker, H., and Sullivan, D.C., "National Cancer Institute iniative: lung image database resource for imaging research," Acad. Radiol. 8(5), 447-450 (2001).
[12] Dodd, L.E., Wagner, R.F., Armato, S.G. III, McNitt-Gray, M.F., Beiden, S., Chan, H.P., Gur, D., McLennan, G., Metz, C.E., Petrick, N., Sahiner, B., and Sayre, J., "Assessment methodologies and statistical issues for computer-aided diagnosis of lung nodules in computer tomography: contemporary research topics relevant to the lung image database consortium," Acad. Radiol. 11(4), 462-475 (2004).
[13] Armato, S.G. III, McNitt-Gray, M.F., Reeves, A.P., Meyer, C.R., McLennan, G., Aberle, D.R., Kazerooni, E.A., MacMahon, H., van Beek, E.J., Yankelevitz, D., Hoffman, E.A., Henschke, C.I., Roberts, R.Y., Brown, M.S., Engelmann, R.M., Pais, R.C., Piker, C.W., Qing, D., Kocherginsky, M., Croft, B.Y., and Clarke, L.P., "The Lung Image Database Consortium (LIDC): an evaluation of radiologist variability in the identification of lung nodules on CT scans," Acad. Radiol. 14(11), 409-421 (2007).
[14] Henschke, C.I., McCauley, D.I., Yankelevitz, D.F., Naidich, D.P., McGuinness, G., Miettinen, O.S., Libby, D., Pasmantier, M., Koizumi, J., Altorki, N., and Smith, J.P., "Early Lung Cancer Action Project: a summary of the findings on baseline screening," Oncologist 6(2), 147-152 (2001).
[15] Reeves, A.P., Biancardi, A.M., Apanasovich, T.V., Meyer, C.R., MacMahon, H., van Beek, E.J.R., Kazerooni, E.A., Yankelevitz, D., McNitt-Gray, M.F., McLennan, G., Armato, S.G. III, Henschke, C.I., Aberle, D.R., Croft, B.Y., and Clarke, L.P., "The Lung Image Database Consortium (LIDC): a comparison of different size metrics for pulmonary nodule measurements," Acad. Radiol. 14(12), 1475-1485 (2007).
[16] de Hoop, B., Gietema, H., van Ginneken, B., Zanen, P., Groenewegen, G., and Prokop, M., "A comparison of six software packages for evaluation of solid lung nodules using semi-automated volumetry: what is the minimum increase in size to detect growth in repeated CT examinations," Eur. Radiol. 19(4), 800-808 (2009).
[17] Zhang, X., Olcott, E., Raffy, P., Yu, N., and Chui, H., "Simulating solid lung nodules in MDCT images for CAD evaluation: modeling, validation, and applications," Proc. SPIE 6514, 65140Z.1-65140Z.8 (2007).
[18] Li, X., Samei, E., DeLong, D.M., Jones, R.P., Gaca, A.M., Hollingsworth, C.L., Maxfield, C.M., Carrico, C.W.T., and Frush, D.P., "Three-dimensional simulation of lung nodules for paediatric multidetector array CT," Br. J. Radiol. 82, 401-411 (2009).
[19] Shin, H.O., Blietz, M., Frericks, B., Baus, S., Savellano, D., and Galanski, M., "Insertion of virtual pulmonary nodules in CT data of the chest: development of a software tool," Eur. Radiol. 16(11), 2567-2574 (2006).

[20] Revel, M.P., Lefort, C., Bissery, A., Bienvenu, M., Aycard, L., Chatellier, G., and Frija, G., "Pulmonary nodules: preliminary experience with three-dimensional evaluation," Radiology 231(2), 459-466 (2004).
[21] Kostis, W.J., Reeves, A.P., Yankelevitz, D.F., and Henschke, C.I., "Three-dimensional segmentation and growth-rate estimation of small pulmonary nodules in helical CT images," IEEE Trans. Med. Imag. 22(10), 1259-1274 (2003).
[22] Ambrosini, R., Wang, P., and O'Dell, W.G., "Volume change determination of metastatic lung tumors in CT images using 3-D template matching," Proc. SPIE 7260, 726035 (2009).
[23] Wang, P., DeNunzio, A., Okunieff, P., and O'Dell, W.G., "Lung metastases detection in CT images using 3D template matching," Med. Phys. 34(3), 915-922 (2007).
[24] McNitt-Gray, M.F., Armato, S.G. III, Meyer, C.R., Reeves, A.P., McLennan, G., Pais, R.C., Freymann, J., Brown, M.S., Engelmann, R.M., Bland, P.H., Laderach, G.E., Piker, C., Guo, J., Towfic, Z., Qing, D.P., Yankelevitz, D.F., Aberle, D.R., van Beek, E.J., MacMahon, H., Kazerooni, E.A., Croft, B.Y., and Clarke, L.P., "The Lung Image Database Consortium (LIDC) data collection process for nodule detection and annotation," Acad. Radiol. 14(12), 1464-1474 (2007).